

Anisotropic Metallic Microlattice Structures for Underwater Operations

Chen Shen, Charles Rohde, Colby W. Cushing, Junfei Li, Zheng Jie Tan, Huifeng Du, Xiuyuan Peng, Preston S. Wilson, Michael R. Haberman, Nicholas X. Fang, and Steven A. Cummer*

Metamaterials have offered unprecedented potentials for wave manipulations. However, their applications in underwater acoustic wave control have remained largely unexplored. This is because of the limited material choices and the lack of reliable fabrication techniques for the complicated structures. Herein, a metamaterial with microlattice structures as the building blocks is proposed for underwater operations. By designing the building blocks of the metamaterial and assembling them in a layered fashion, anisotropy is embedded in the structure, which results along different effective sound speeds in orthogonal directions. The designed metamaterial is fabricated by metal additive manufacturing using aluminum and steel. Experiments are performed using a resonator tube to evaluate its performance in water. An anisotropy ratio of around 2 is achieved, which is in good agreement with numerical simulations. The proposed metamaterial provides an effective means for underwater sound control with reduced fabrication difficulties and increased service life.

1. Introduction

The advent of metamaterials has enabled a plethora of devices with intriguing wave engineering capabilities.^[1–3] Despite their great success in optics, acoustics, and mechanics, their usefulness in underwater applications has been less explored. Designing acoustic metamaterials for underwater operations, on the other hand, is meaningful for a number of applications including sensing, communication, and noise control.^[4–13] Compared with their utilization in the air, underwater metamaterials face several challenges. As the structure needs to be placed in water for effective operations, the constituent materials need to be chosen carefully to be long-durable under harsh environments. Moreover, typical materials used in water have similar

characteristic impedance as the background medium. The lack of high impedance contrast makes it difficult to directly bring strategies such as space-coiling^[14] and resonator-based structures^[15,16] used in the air into the underwater domain. The limited material choices in turn pose challenges to reliable manufacturing of the metamaterials.

Another difficulty to design and realize underwater metamaterials is the complex solid–fluid interactions, which can result in complicated structures to account for the vibration of the solid parts. For example, it has been shown that the control of shear modulus is crucial for underwater metamaterials, as the coupling of pressure and shear waves can result in undesired resonances which could degrade their performance.^[17–19] One option is to use pentamode metamaterials which are composed of latticed filaments with solid inclusions.^[20–25] These metamaterials can effectively handle interactions with dense fluids and reduce shear modulus, but contain delicate structures and inclusions that are difficult to manufacture. Another solution is to surround the solid materials with background fluid or connect them with soft materials.^[19,26] However, one should be careful in choosing the right connection technique to avoid mechanical instability. The recent development of metal additive manufacturing has brought about new possibilities in the design and fabrication of metamaterials, especially using strong materials such as metal.^[27,28] Such advanced manufacturing techniques are capable to build cellular solids with high precision, which offer great flexibility to realize metallic structures with engineered properties.^[29,30]


C. Shen, J. Li, X. Peng, S. A. Cummer
Department of Electrical and Computer Engineering
Duke University
Durham, NC 27708, USA
E-mail: cummer@duke.edu

C. Shen
Department of Mechanical Engineering
Rowan University
Glassboro, NJ 08028, USA

C. Rohde
Acoustics Division
U.S. Naval Research Laboratory
Code 7165, Washington, DC 20375, USA

C. W. Cushing, P. S. Wilson, M. R. Haberman
Applied Research Laboratories and Walker Department of Mechanical Engineering
The University of Texas at Austin
Austin, TX 78713-8029, USA

Z. J. Tan, H. Du, N. X. Fang
Department of Mechanical Engineering
Massachusetts Institute of Technology
Cambridge, MA 02139, USA

 The ORCID identification number(s) for the author(s) of this article can be found under <https://doi.org/10.1002/adem.202201294>.

DOI: 10.1002/adem.202201294

In this article, we present a metamaterial consisting of layered microlattice structures and steel sheets for underwater operations. We consider general underwater applications and neglect the effect of water pressure, which could be significant in deep-water environments. The microlattice structures can be engineered to be anisotropic. Together with a layered arrangement of steel sheets connected by soft rubber rods, the metamaterial exhibits anisotropic mass density and a sufficiently reduced shear modulus. The metamaterial is fabricated using metal additive manufacturing techniques using aluminum and steel. Experiments are performed and the results are in good agreement with numerical predictions. In addition, it is found that metal additive manufacturing of cellular solids could lead to degraded mechanical strength compared with bulk counterparts, evidenced by acoustic measurements. The proposed metamaterial with built-in anisotropy and strong mechanical stiffness can be useful in underwater wave control, especially in directional control of wave propagation and designing devices based on transformation acoustics.

2. Design and Numerical Simulations

The structure of the proposed metamaterial is depicted in **Figure 1**. The truss elements have a diameter of 1 mm and are arranged at 45° to form a cubic architecture before being rescaled. The unit cell of the metallic slab is microlattice structures composed of octet truss elements.^[31,32] These structures are capable of delivering high mechanical stiffness and lightweight, which are preferred in underwater sound control to provide small density and good impedance matching. Here, the microlattice structures are modified to be compatible with additive manufacturing techniques. Namely, the vertical truss elements are removed so that no overhanging structures are in place by properly orienting the parts during fabrication. The unit cell is then rescaled to be asymmetric as illustrated in **Figure 1a**. It will be shown that these modifications result

in the reliable manufacturing of the structures. Moreover, the asymmetric unit cell leads to built-in anisotropy of the metallic slabs, as will be confirmed by numerical simulations. An improved acoustic property may be obtained by further optimizing the microlattice architecture of the unit cells. It should be noted that, however, compared with metamaterials that work in the air whose constituent materials are typically considered acoustically rigid, it is more challenging to design underwater metamaterials as fluid–solid interactions need to be considered. The geometric asymmetry is tuned so that the metamaterials display anisotropic acoustic properties while being compatible with the fabrication process. By integrating the slabs with steel sheets, the metamaterial exhibits a high degree of anisotropy, which is highly demanded in designing devices that exhibit different properties along different directions. To reduce the shear modulus of the assembled metamaterial, here we use soft rubber rods, which are secured in position by the slots on the slabs.^[33]

To this end, numerical simulations based on finite element analysis are performed to analyze the effective properties of the metamaterial. As each metamaterial slab contains 6-by-6 octet truss elements, it is time-consuming to simulate the entire structure directly. To reduce the computational load, we adopt a two-step simulation approach^[34] to extract the effective parameters of the proposed metamaterial. The first step is to conduct simulations for a slab of the microlattice structures as shown in **Figure 1b**. The simulation setup in this step is depicted in **Figure 2a,b**, where explicit inner structures and full solid–fluid couplings are considered to best capture the response of the structure. The retrieved parameters will then be plugged into the next step to study the properties of the assembled structure (**Figure 1c**) and the slabs will be modeled as effective media for better computational efficiency.

Figure 2c,d shows the extracted effective density and sound speed in the perpendicular and parallel directions for a slab of the microlattice structures using aluminum. The perpendicular direction is defined as waves propagating perpendicular to the

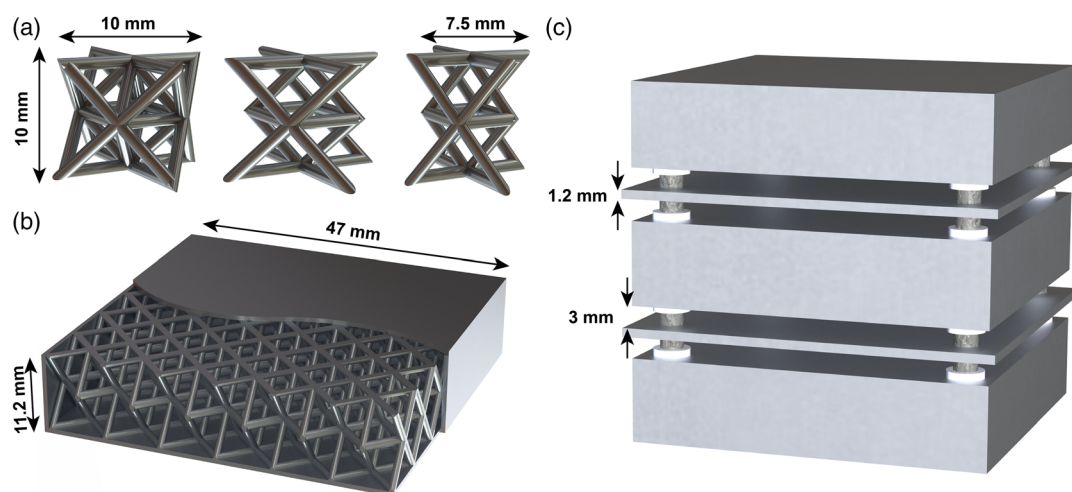


Figure 1. Geometry of the underwater metamaterial. a) Evolution of the unit cell. Left: unit cell with octet truss elements. Middle: the vertical truss elements are removed for reliable additive manufacturing. Right: the unit cell is rescaled to induce anisotropy. b) A sealed plate structure containing the modified unit cells. c) Metamaterial assembly using a layered structure with steel plates and soft connections. Please confirm that forenames/given names (blue), surnames/family names (vermilion), and corresponding author(s) (asterisk) have been identified correctly.

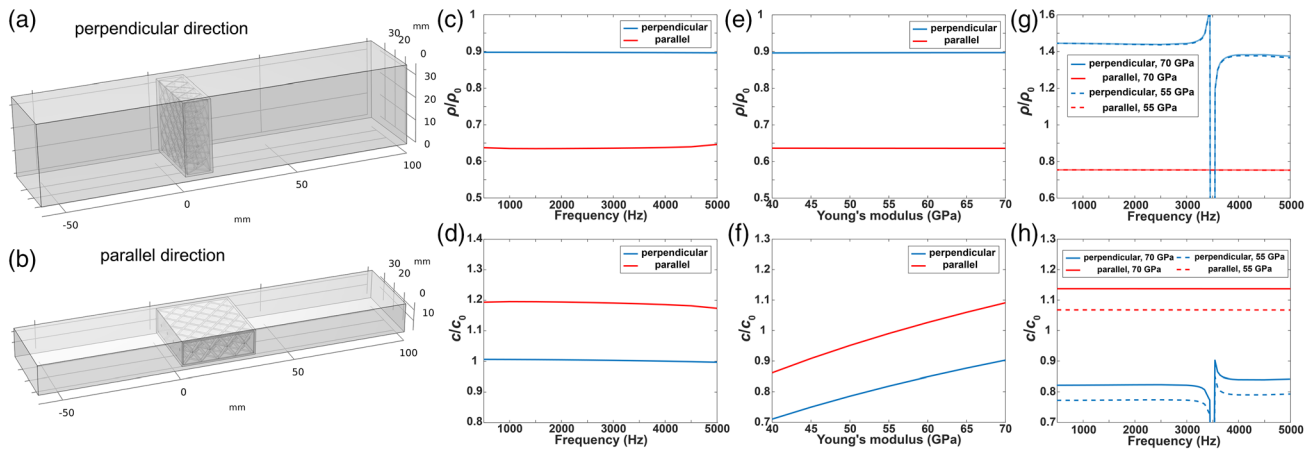


Figure 2. Effective properties of the underwater metamaterial. a,b) Simulation setup to extract the effective properties in perpendicular and parallel directions using an accurate representation of the inner structures of a microlattice slab. c,d) Effective density and sound speed of the microlattice slab with original Young's modulus (70 GPa) as a function of frequency. e,f) At 3000 Hz, the effective density and sound speed change by assigning different Young's moduli to the constituent material. g,h) The assembled metamaterial exhibits a higher degree of anisotropy in terms of its effective density and sound speed. The curves are obtained from the original Young's modulus (70 GPa) and a reduced one at 55 GPa.

microlattice slabs. Thanks to the rescaling of the core structure, the slab exhibits some degree of anisotropy. It should be noted that, while we used the original Young's modulus of aluminum (70 GPa) in the simulation, the actual stiffness of the manufactured material can be degraded. This deterioration is common for structures fabricated by additive manufacturing.^[35–37] To study this, we varied the Young's modulus of the constituent material and calculated its effect on the effective acoustic parameters. The results are summarized in Figure 2e,f at a frequency of 3000 Hz. Interestingly, the effective density remains almost the same regardless of the change of the Young's modulus. The effective sound speed, on the other hand, depends heavily on the stiffness of the constituent material and increases monotonically as a function of the Young's modulus. These findings can be used as a criterion to analyze the deterioration of the fabricated parts, as will be discussed later in the experiment section. By integrating with steel sheets to form an assembled metamaterial unit cell (Figure 1c), the degree of anisotropy is increased and the ratio of the effective density in the orthogonal directions approaches two, as can be seen from Figure 2g,h. Similar to the results obtained from the slab, the effective densities remain unaltered for two different Young's moduli at 70 and 55 GPa. The effective sound speeds decrease for degraded stiffness, implying a reduced bulk modulus. A narrow-band resonance is observed around 3500 Hz in the perpendicular direction, which decreases the usable bandwidth of the metamaterial. The resonance could be caused by the interaction between the steel sheets and is typical for such arrangements.^[19] Nevertheless, the results clearly show that the designed metamaterial exhibits a moderate anisotropic response, which is crucial in controlling underwater acoustic waves. Moreover, compared with previous approaches using periodically arranged metallic plates where the effective density is always above unity, the metamaterial we proposed achieves subunity density. This leads to better impedance matching ($Z = \rho c$) with the background medium and is preferred in applications including acoustic

focusing and cloaking. The corresponding data for metamaterials using steel exhibit a similar trend and display an anisotropic density ratio of around 1.5 (Figure S1, Supporting Information).

3. Fabrication and Experimental Characterization

As the proposed metamaterial consists of microlattice structures containing thin truss elements, it is difficult to realize it using conventional manufacturing approaches. In this work, we employ metal additive manufacturing techniques to fabricate the plate structures.^[27,38,39] The enclosed metallic lattices were fabricated using selective laser melting (SLM) on a GE Additive M2 Cusing system. For steel samples, this approach uses a layer-by-layer melting of stock stainless steel 316L powder into a solid part supported against gravity during sintering by the surrounding unsintered powder. Aluminum samples are fabricated in the same manner. Because fully unsupported elements cannot be processed with this method, overhanging trusses must be supported with additional sintered material. The limited access to the interstitial space of the enclosed lattice structure precludes adding supporting elements. This limits the design space, requiring the avoidance of truss elements with overhangs greater than 45° from the build plate surface normal. Therefore, the vertical trusses are removed to facilitate the fabrication process, as discussed in the previous section. The thin-walled enclosing box serves both, as a water barrier during use and as an external support structure for the SLM approach. These walls anchor the internal lattice against thermally induced warping during the high thermal gradient build process. The top of the supporting box is left open to allow for the removal of the unsintered metal powder. The top is built as a separate element, next to the lattice structure. The fabricated building block is then sealed and connected to steel sheets using soft rubber rods. **Figure 3** shows the fabricated microlattice structures and the assembled metamaterials. Additional details of the build process can be found in the supporting materials.

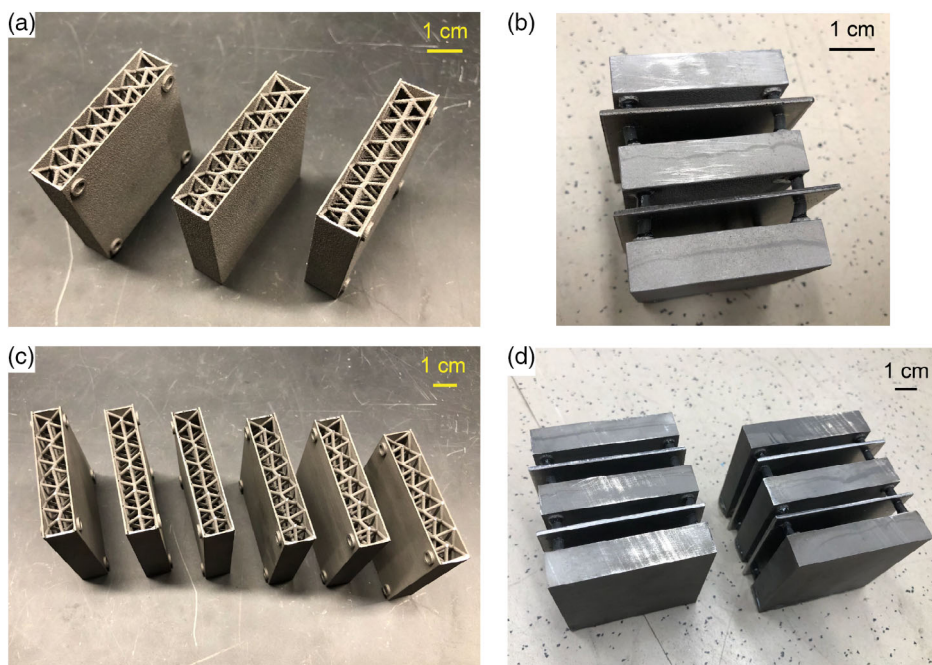


Figure 3. Fabrication of the metamaterial. a,b) Additive manufacturing of the microlattice structure using aluminum and the assembled metamaterial structure. c,d) Additive manufacturing of the microlattice structure using steel and the assembled metamaterial structure.

To experimentally characterize the proposed metamaterial, measurements were carried out based on a resonator tube waveguide approach.^[34] The experimental setup is shown in **Figure 4**. The resonator tube is a glass-walled tube with a 5.28 cm radius and 0.615 m length and is filled with fresh degassed water. The resonator tube is excited by a chirp signal with a frequency of 0.05–10 kHz using a piston and the response is recorded by a

hydrophone (model Brüel & Kjær 8103). The frequency-dependent acoustic response of the system, which is the measured acoustic pressure normalized by the drive signal, is obtained by calculating the transfer function between the hydrophone signal and the drive signal. The tube has an air–water interface at the top and a Styrofoam layer on the bottom surface which can both be approximated as pressure release boundary

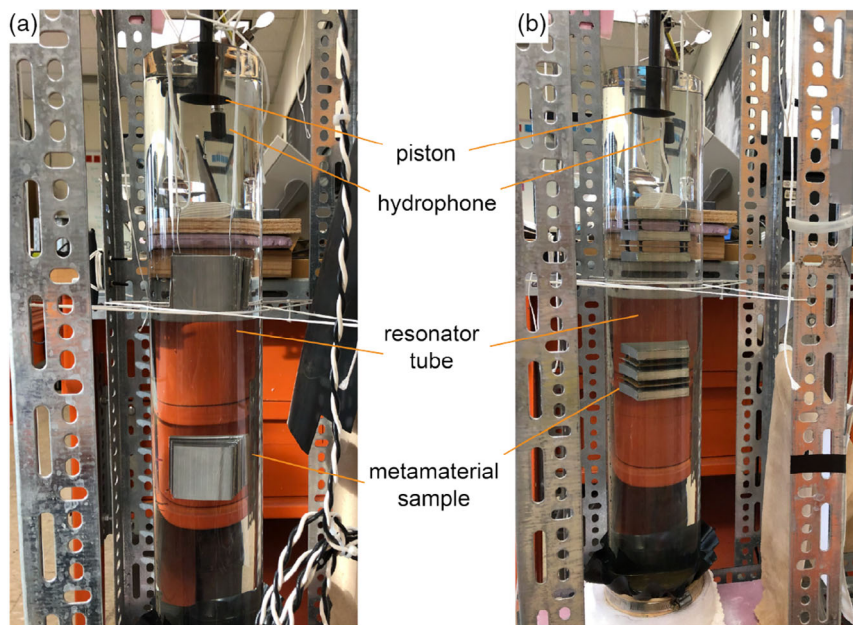


Figure 4. Experimental setup of the resonator tube to characterize the underwater metamaterial. a) Parallel configuration. b) Perpendicular configuration.

conditions. The organ-pipe-like resonances will therefore occur at integer multiples of half wavelengths. The peaks in the system responses represent standing wave resonances of plane wave-like modes. For example, Figure 6a shows the measured system response of a water-filled tube without samples. The metamaterials immersed in the resonator tube will affect the effective sound speed exhibited by the system, which further leads to a resonance frequency shift in the system response. By further reorienting the metamaterials, their properties along parallel and perpendicular directions can be inferred. An analytical material properties extraction method has been used, based on the theoretical approach outlined by Laffleur and Shields^[40] and the details can be found in ref. [34]. Here, a purely numerical method of material properties extraction is done in the finite-element domain. In the following, we discuss the results and characterization of additively manufactured aluminum samples in the main text while details regarding the steel samples are presented in the supporting materials.

As mentioned above, the fabricated metamaterial may have induced a certain deterioration in terms of the stiffness of the constituent metal. To evaluate this effect, the experimental spectra are compared with spectra from a finite-element simulation of the water- and metamaterial-filled resonator tube. In the finite element model, the effective density and sound speed obtained from the assembled metamaterial are used to reduce computational load.^[34] In the measurements, the system response of the resonator tube represents resonance frequencies due to the effective sound speed of the metamaterial–water mixture inside the tube. The effective properties of the metamaterial are dependent upon the microlattice structure, which in turn is dependent on the Young’s modulus of the 3D printed material. In this manner, the Young’s modulus of the structures after fabrication can be determined by finding the best fit with the experimental results. We first estimate the acoustic properties of the assembled metamaterial as a function of the Young’s modulus of the constituent material, as shown in Figure 5a,b. Because of the relatively weak dispersion (Figure 2g,h), these properties are calculated at a fixed frequency of 3000 Hz for comparison. Then the extracted acoustic properties are inserted into the finite-element model that contains the resonator tube to determine the best fit with the experimental results. The relative difference is extracted by comparing the frequency of the first five resonance peaks between simulation and measurement and is defined as

$$\Delta = \sqrt{\sum_{i=1}^5 (f_s^i - f_m^i)^2} \quad (1)$$

where f_s^i and f_m^i denote the i th resonance peak in simulation and measurement, respectively. The results are plotted in Figure 5c where the smallest relative difference occurs at a reduced Young’s modulus at 50 and 55 GPa for perpendicular and parallel directions, respectively. The slight discrepancy between the two directions is likely to be caused by measurement uncertainties. Nevertheless, the trends in both directions suggest that the 3D printed material is experiencing a degradation because the original stiffness value does not produce the best agreement. The overall simulated and measured system response along parallel and perpendicular directions is summarized in Figure 6b,c at a Young’s modulus of 55 GPa, with the zoom-in view of the second, third, and fourth peaks depicted in Figure 6d–f. The measured peaks, which denote resonance frequencies at different situations, are well captured by the numerical simulations. The agreement is better with this reduced stiffness as compared to the original value at 70 GPa, confirming the existence of structural deterioration during fabrication (Figure S2, Supporting Information). The final acoustic properties normalized by those of water with fitted Young’s modulus are found to be $\rho_{\perp} = 1.441$, $\rho_{\parallel} = 0.754$ and $c_{\perp} = 0.771$, $c_{\parallel} = 1.067$. The metamaterial exhibits an anisotropy ratio of around 2 in terms of effective density, which is meaningful for underwater operations that require anisotropic properties. Notably, this anisotropy ratio is about a 40% enhancement compared to the original microlattice slab and could be further increased by increasing the filling ratio of the steel sheets.^[19] The simulated and experimentally obtained results for steel samples demonstrate a similar manner, with an estimated reduced Young’s modulus of 140 GPa as compared to 205 GPa (Figure S3–S5, Supporting Information).

4. Conclusion

We have designed a metallic metamaterial for underwater operations. The building block incorporates anisotropic microlattice structures and, by further integrating with parallel steel sheets, yields anisotropic mass densities in orthogonal directions. In addition, the density in the parallel direction

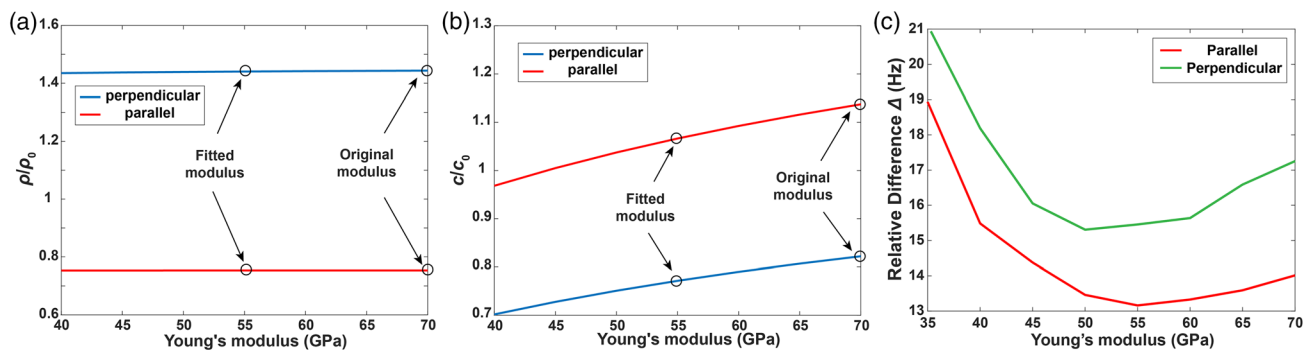


Figure 5. Effect of different Young’s modulus of the constituent material. a,b) Effective density and sound speed of the assembled metamaterial. c) Relative difference between simulated and measured resonance peaks.

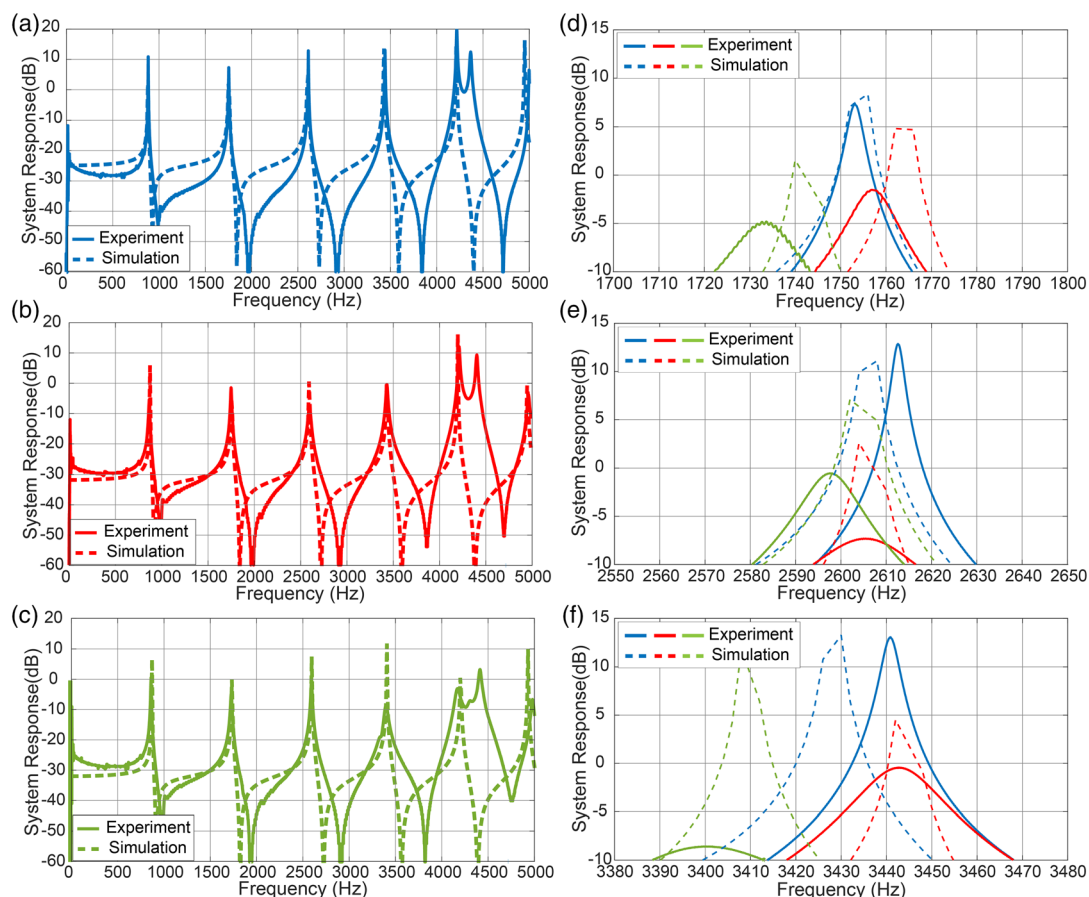


Figure 6. Measured and simulated system responses of the three different resonator tube assemblies for additively manufactured aluminum samples. a) Water-only case (no metamaterial). b) Parallel direction. c) Perpendicular direction. d–f) Zoom-in view of the second, third, and fourth peaks to illustrate the shift of resonance frequencies in different orientations.

can be designed to be subunity, which leads to better impedance matching with the background medium. The structure is mechanically robust and can be fabricated reliably using metal additive manufacturing. Measurements performed in a water tube confirmed the validity of the numerical approach and the effectiveness of the metamaterial. Notably, it is found that the mechanical stiffness of the printed material is reduced during the process of additive manufacturing and this effect is captured by acoustic measurements. The results imply that structural degradation needs to be taken into consideration in designing metallic cellular materials using 3D printing.

Compared with previous underwater metamaterials composed of parallel plates and pentamode structures, the metamaterial we proposed can help achieve larger anisotropy with a relatively simple configuration that can be fabricated conveniently via additive manufacturing. The good impedance matching also makes it ideal for underwater sound control,^[41] especially in devices designed by transformation acoustics. Recently, bubbly media have also been proposed as a unit cell architecture for the design of underwater metamaterials.^[10,42,43] These structures host strong resonances that can lead to extreme effective properties. However, they are more fragile and may not be used in applications that require long-term stability and

duration in harsh environments. We hope the proposed metamaterial as well as the design and manufacturing approach will open new avenues for the design and application of underwater metamaterials.

Supporting Information

Supporting Information is available from the Wiley Online Library or from the author.

Acknowledgements

This work was supported by a Multidisciplinary University Research Initiative grant from the Office of Naval Research (grant no. N00014-13-1-0631) and an Emerging Frontiers in Research and Innovation grant from the National Science Foundation (grant no. 1641084).

Conflict of Interest

The authors declare no conflict of interest.

Data Availability Statement

The data that support the findings of this study are available from the corresponding author upon reasonable request.

Keywords

additive manufacturing, anisotropy, metal 3D printing, microlattice structures, underwater metamaterials

Received: September 19, 2022

Revised: November 3, 2022

Published online: November 22, 2022

- [1] N. Engheta, R. W. Ziolkowski, *Metamaterials: Physics and Engineering Explorations*, John Wiley & Sons, Hoboken, NJ, USA **2006**.
- [2] S. A. Cummer, J. Christensen, A. Alù, *Nat. Rev. Mater.* **2016**, *1*, 16001.
- [3] K. Bertoldi, V. Vitelli, J. Christensen, M. van Hecke, *Nat. Rev. Mater.* **2017**, *2*, 17066.
- [4] C. J. Naify, T. P. Martin, C. N. Layman, M. Nicholas, A. L. Thangawng, D. C. Calvo, G. J. Orris, *Appl. Phys. Lett.* **2014**, *104*, 073505.
- [5] C. Shen, J. Xu, N. X. Fang, Y. Jing, *Phys. Rev. X* **2014**, *4*, 041033.
- [6] T. Brunet, A. Merlin, B. Mascaro, K. Zimny, J. Leng, O. Poncelet, C. Aristégui, O. Mondain-Monval, *Nat. Mater.* **2015**, *14*, 384.
- [7] A. J. Hicks, M. R. Haberman, P. S. Wilson, *J. Acoust. Soc. Am.* **2015**, *138*, EL254.
- [8] C. Shi, M. Dubois, Y. Wang, X. Zhang, *Proc. Natl. Acad. Sci.* **2017**, *114*, 7250.
- [9] X. Jiang, B. Liang, J. C. Cheng, *Adv. Mater.* **2018**, *30*, 1800257.
- [10] Z. Cai, S. Zhao, Z. Huang, Z. Li, M. Su, Z. Zhang, Z. Zhao, X. Hu, Y.-S. Wang, Y. Song, *Adv. Funct. Mater.* **2019**, *29*, 1906984.
- [11] L. Tong, Z. Xiong, Y. X. Shen, Y. G. Peng, X. Y. Huang, L. Ye, M. Tang, F.-Y. Cai, H.-R. Zheng, J.-B. Xu, G. J. Cheng, X.-F. Zhu, *Adv. Mater.* **2020**, *32*, 2002251.
- [12] S. Qu, N. Gao, A. Tinel, B. Morvan, V. Romero-García, J. P. Groby, P. Sheng, *Sci. Adv.* **2022**, *8*, eabm4206.
- [13] K. Wu, J. J. Liu, Ding Yj, W. Wang, B. Liang, J. C. Cheng, *Nat. Commun.* **2022**, *13*, 5171.
- [14] R. Ghaffarivardavagh, J. Nikolajczyk, R. G. Holt, S. Anderson, X. Zhang, *Nat. Commun.* **2018**, *9*, 1349.
- [15] L. Huang, Y. K. Chiang, S. Huang, C. Shen, F. Deng, Y. Cheng, B. Jia, Y. Li, D. A. Powell, A. E. Miroshnichenko, *Nat. Commun.* **2021**, *12*, 4819.
- [16] T. Yang, Z. Lin, T. Yang, *Adv. Eng. Mater.* **2022**, 2200805, <https://doi.org/10.1002/adem.202200805>.
- [17] Y. Urzhumov, F. Ghezzi, J. Hunt, D. R. Smith, *New J. Phys.* **2010**, *12*, 073014.
- [18] J. D. Smith, P. E. Verrier, *Proc. R. Soc. A* **2011**, *467*, 2291.
- [19] B. I. Popa, W. Wang, A. Konneker, S. A. Cummer, C. A. Rohde, T. P. Martin, G. J. Orris, M. D. Guild, *J. Acoust. Soc. Am.* **2016**, *139*, 3325.
- [20] A. N. Norris, *J. Acoust. Soc. Am.* **2009**, *125*, 839.
- [21] C. N. Layman, C. J. Naify, T. P. Martin, D. C. Calvo, G. J. Orris, *Phys. Rev. Lett.* **2013**, *111*, 024302.
- [22] M. Kadic, G. W. Milton, M. van Hecke, M. Wegener, *Nat. Rev. Phys.* **2019**, *1*, 198.
- [23] H. W. Dong, S. D. Zhao, X. B. Miao, C. Shen, X. Zhang, Z. Zhao, C. Zhang, Y.-S. Wang, L. Cheng, *J. Mech. Phys. Solids* **2021**, *152*, 104407.
- [24] C. W. Cushing, M. J. Kelsten, X. Su, P. S. Wilson, M. R. Haberman, A. N. Norris, *J. Acoust. Soc. Am.* **2022**, *151*, 168.
- [25] A. Zhao, H. Jia, M. Zhang, Z. Wang, P. Zhou, C. Liu, Z. Zhao, X. Zhang, T. Wu, H. Chen, B. Liu, B. Song, *Phys. Rev. Appl.* **2022**, *18*, 034001.
- [26] Y. Bi, H. Jia, Z. Sun, Y. Yang, H. Zhao, J. Yang, *Appl. Phys. Lett.* **2018**, *112*, 223502.
- [27] W. E. Frazier, *J. Mater. Eng. Perform.* **2014**, *23*, 1917.
- [28] M. Askari, D. A. Hutchins, P. J. Thomas, L. Astolfi, R. L. Watson, M. Abdi, M. Ricci, S. Laureti, L. Nie, S. Freear, R. Wildman, C. Tuck, M. Clarke, E. Woods, A. T. Clare, *Addit. Manuf.* **2020**, *36*, 101562.
- [29] O. Rahman, K. Z. Uddin, J. Muthulingam, G. Youssef, C. Shen, B. Koohbor, *Adv. Eng. Mater.* **2022**, *24*, 2100646.
- [30] A. du Plessis, S. M. J. Razavi, M. Benedetti, S. Murchio, M. Leary, M. Watson, D. Bhate, F. Berto, *Prog. Mater. Sci.* **2022**, *125*, 100918.
- [31] X. Zheng, H. Lee, T. H. Weisgraber, M. Shusteff, J. DeOtte, E. B. Duoss, J. D. Kuntz, M. M. Biener, Q. Ge, J. A. Jackson, S. O. Kucheyev, N. X. Fang, C. M. Spadaccini, *Science* **2014**, *344*, 1373.
- [32] J. Feng, B. Liu, Z. Lin, J. Fu, *Mater. Des.* **2021**, *203*, 109595.
- [33] C. W. Cushing, P. S. Wilson, M. R. Haberman, C. Shen, S. Cummer, *J. Acoust. Soc. Am.* **2019**, *145*, 1727.
- [34] C. W. Cushing, P. S. Wilson, M. R. Haberman, C. Shen, J. Li, S. A. Cummer, Z. J. Tan, C. Ma, H. Du, N. X. Fang, *J. Acoust. Soc. Am.* **2021**, *149*, 1829.
- [35] C. Shuai, Y. Cheng, Y. Yang, S. Peng, *J. Alloys Compd.* **2019**, *798*, 606.
- [36] J. P. Oliveira, A. LaLonde, J. Ma, *Mater. Des.* **2020**, *193*, 108762.
- [37] A. M. Roach, B. C. White, A. Garland, B. H. Jared, J. D. Carroll, B. L. Boyce, *Addit. Manuf.* **2020**, *32*, 101090.
- [38] J. J. Lewandowski, M. Seifi, *Annu. Rev. Mater. Res.* **2016**, *46*, 151.
- [39] N. Haghdadi, M. Laleh, M. Moyle, S. Primig, *J. Mater. Sci.* **2021**, *56*, 64.
- [40] L. D. Lafleur, F. D. Shields, *J. Acoust. Soc. Am.* **1995**, *97*, 1435.
- [41] H. W. Dong, S. D. Zhao, M. Oudich, C. Shen, C. Zhang, L. Cheng, Y.-S. Wang, D. Fang, *Phys. Rev. Appl.* **2022**, *17*, 044013.
- [42] T. Lee, H. Iizuka, *Phys. Rev. B* **2020**, *102*, 104105.
- [43] C. Choi, S. Bansal, N. Münzenrieder, S. Subramanian, *Adv. Eng. Mater.* **2021**, *23*, 2000988.